*Highlights (for review)

- MAR and ENR fluoroquinolones (FQs) sorption on sepiolite was studied in water
- S-logistic 1 sigmoidal model best fits experimental data for both FQs
- Solid-state photodegradation of FQs adsorbed on sepiolite was tested
- Sunlight-induced photodegradation profiles over irradiation time were traced

Removal of fluoroquinolone contaminants from water on sepiolite and its photo-induced regeneration

Michela Sturini[*a], Andrea Speltini [a], Federica Maraschi [a], Antonella Profumo [a], Serena Tarantino[c], Alessandro F. Gualtieri [b], Michel Zema[c]

[a]Department of Chemistry, University of Pavia, via Taramelli 12, 27100 Pavia, Italy

[b]Department of Chemical and Earth Sciences, University of Modena and Reggio Emilia, Via Campi 103, 41125 Modena, Italy

[c]Department of Earth and Environmental Sciences, University of Pavia, via Ferrata 9, 27100 Pavia, Italy

[*]Corresponding author. Tel.: +39 0382 987347; fax: +39 0382 528544.

E-mail: michela.sturini@unipv.it (M. Sturini)

Abstract

In this work, sepiolite is studied as a sorbent phase for the removal of Fluoroquinolone (FQ) contaminants from water. Marbofloxacin (MAR) and Enrofloxacin (ENR) were chosen as model FQs since they are the two most commonly employed veterinary FQs in livestock farming in northern Italy. Adsorption experiments on two sepiolites (SP-1 and SSE16) were carried out in tap water at pH 7.5 to better mimic real conditions. Adsorption isotherms were determined by fitting the experimental data by the Freundlich, Langmuir and S-Logistic1 models. The last better described MAR and ENR adsorptions. Adsorption capacities of SP-1 and SSE16, respectively, were 132 mg g^{-1} and 121 mg g^{-1} for MAR, and 112 mg g^{-1} and 93 mg g^{-1} for ENR. X-ray powder diffraction, performed on clay samples enriched with each FQ and for comparison on the pristine clays, showed no substantial differences between the two sepiolites and evidenced no significant structural changes after FQs uptake, as also verified by infrared spectroscopy. This indicates that the adsorption occurs only on the external surface of the mineral and not in the intracrystalline microporosity, likely due to the interaction between the FQ carboxylic group and the Mg^{2+} ions present on the sepiolite surface. Solid-state photodegradation of the adsorbed FQs, not presently studied on sepiolite materials, was also investigated for regenerating the sorbent once recovered from water. Results showed that

the adsorbed drugs are effectively photodegraded by solar light irradiation (outdoor conditions), thus allowing the sepiolite to be recycled for further remediation of contaminated water.

Keywords: Emerging pollutants; Fluoroquinolones; Photodegradation; Remediation; Sepiolite; Adsorption.

1. Introduction

The occurrence, behaviour and fate of pharmaceutically active compounds in the environment are attracting great attention in the field of environmental sciences. In particular, Fluoroquinolones (FQs) represent one of the main classes of emerging pollutants due to their ubiquitous presence in water and soil systems (Andreu et al., 2007; Speltini et al., 2010; Speltini et al., 2011). FQs are zwitterionic molecules obtained by modification of the quinolone core structure by insertion of a fluorine atom in C-6 position and a piperazinyl – or piperazine derivative – group at C-7. FQs are largely used both in human and veterinary medicine in reason of their high potency, broad activity spectrum, good bioavailability, high serum levels, and potentially low side-effects incidence (Andersson and MacGowan, 2003).

These antibiotics are only partially metabolised, thus large part of the ingested dose (>50%) is excreted with no structural modification (Reemtsma and Jekel, 2006; Van Doorslaer et al., 2011). From the environmental point of view, the poor metabolization stands for the release of variable amounts of pharmaceutically active FQs through wastewater, as the actual treatment plants are not capable of quantitative abatement. In fact, FQs have been frequently quantified in environmental waters at concentrations ranging from ng L^{-1} to μg L^{-1} (Speltini et al., 2010), and in wastewater effluents (Andreozzi et al., 2003). As their main abiotic transformation path, photodegradation is very important to prevent accumulation of these otherwise persistent compounds (Andreozzi et al., 2003; Speltini et al., 2010; Sturini et al., 2014). Nevertheless, since full mineralization is hard to achieve under actual environmental conditions (Kusari et al., 2009), variable amounts of parent drugs together with their photoproducts are present in water systems (Babić et al., 2013; Prabhakaran et al., 2009; Sturini et al., 2010; Sturini et al., 2014). Recent works gave evidence that photoproducts greatly contribute to the environmental impact of FQs pollution. Indeed, it was proved that some FQs photoproducts retain antimicrobial activity, thus contributing to stimulate bacterial resistance (De

55 Bel et al., 2009; Kusari et al., 2009; Sturini et al. 2012a; Sukul et al. 2009); additionally, different studies
56 reported that significant toxicity is maintained after photolysis of FQs aqueous solutions, due to the
57 formation of bioactive products (Li and Niu et al., 2011; Sirtori et al., 2012; Sturini et al., 2015a;
58 Vasconcelos et al., 2009), and it has been proved that genotoxicity of hospital wastewater was largely
59 attributed to FQs (Hartmann et al., 1998). Moreover, veterinary FQs, as other veterinary drugs, once spread
60 in farm fields through fertilization practices, could enter the food chain via plants uptake (Boxall et al.,
61 2006). As well, the risk of drinking water contaminated by FQs cannot be ruled out, as documented for
62 quinolones (Vieno et al., 2007; Wang et al., 2010; Ye and Weinberg, 2007).
63 It is evident that developing efficient procedures for water decontamination aimed at preventing the
64 widespread of such emerging pollutants is a priority task. Advanced oxidation processes (AOPs) have been
65 proposed for pharmaceuticals abatement – including FQs – from wastewaters, but poor information is
66 available about their effectiveness and anyway result to be expensive and not fully environmental friendly
67 (Laera et al., 2012; Lester et al., 2011; Rizzo et al., 2013).
68 The employment of natural materials characterized by high surface area and sorption capacity as adsorbent
69 phases seems an alternative approach for remediation of contaminated aqueous matrices, as proved for
70 montmorillonite, kaolinite and zeolites (Gianotti et al., 2008; Li and Hong et al., 2011; Martucci et al., 2012).
71 Among clay minerals, sepiolite showed great potentiality as sorbent phase for remediation of water
72 contaminated by heavy metals and organics, such as diethylketone (Ghahfarokhi et al., 2014; Quintelas et al.,
73 2011). To the authors' best knowledge, no literature data are currently available on sepiolite as adsorbent for
74 the removal of FQ species from water media.
75 Sepiolite is a trioctahedral phyllosilicate, with theoretical formula $Si_{12}O_{30}Mg_8(OH)_4(OH_2)_4 \cdot 8H_2O$. The
76 structure of this mineral was described by Brauner and Presinger (1956), and is characterized by the
77 presence, along the *c* axis, of channels (4 Å by 9.5 Å), which can hold zeolitic H_2O as well as other small
78 molecules. It differs from laminar clays in that it has a fibrous morphology at microscopic and sometimes
79 macroscopic levels. The fibrous morphology, the presence of intra-crystalline channels as well as the small
80 particles size result in high specific surface area values. The reported values of BET surface area for sepiolite
81 range between ~80 and 350 $m^2\ g^{-1}$ (Nishimura et al., 1972; Suarez and García-Romero, 2012). Due to its

physicochemical properties, especially its surface properties, sepiolite is a clay mineral with a wide range of applications. A review of the industrial uses of sepiolite is given in Murray (1999). Sepiolite is moreover a cheap, fairly abundant and safe solid sorbent. Considering the overall picture of FQs environmental diffusion and the actual state of the art for remediation of FQs-contaminated waters, in this work two sepiolites have been tested to evaluate their adsorption capacity towards FQs: one sepiolite standard (SP-1) has been compared to a low grade sample (SSE16). Adsorption capacities of the two clays have been put in relation with their physical-chemical properties, i.e. surface area, determined by Brunauer–Emmett–Teller (BET), and structural morphology, studied by field emission scanning electron microscopy (FE-SEM). The sorption profiles have been traced and the uptake of the two FQs, Marbofloxacin (MAR) and Enrofloxacin (ENR), has been investigated also by complementary techniques, *viz.* X-ray powder diffraction (XRPD) and Fourier transform infrared attenuated total reflectance (FTIR-ATR), to get information about the sorption mechanism. Photo-induced removal of the adsorbed FQs (solid-state photodegradation) has been also investigated under natural sunlight for regenerating the sorbent once recovered from water.

2. Experimental section

2.1. Reagents and materials

Two samples of sepiolite, SP-1 (50 grm/unit), Valdemore, Spain (Miocene age, contains minor calcite) from the Clay Mineral Society (http://www.clays.org/SOURCE%20CLAYS/SCdata.html) and a second one (SSE16) from Mazzaron Vallecas pits (Spain) were disposable and kindly provided by M. Setti (Department of Earth and Environmental Sciences, University of Pavia). Both materials were used as received, with no further purification.

All the chemicals employed were reagent grade or higher in quality. MAR and ENR, in the injectable form, were purchased from Bayer (Baytril 25 mg mL^{-1}) and Vétoquinol (Marbocyl 20 mg mL^{-1}), respectively. HPLC gradient grade acetonitrile (ACN) was from VWR; H_3PO_4 (85%, w/w) was purchased from Carlo Erba Reagents; 1 M tetrabutyl ammonium hydroxide (TBAH) was from Sigma-Aldrich.

Ultra-pure water (resistivity 18.2 MΩ cm^{-1} at 25°C) was produced by a Millipore (Milan, Italy) Milli-Q system. FQs stock solutions were prepared and stored in the dark at 4°C for a maximum of three months. Working solutions were renewed weekly.

2.2. Adsorption experiments

FQ adsorption on sepiolite was studied using a batch equilibration method. Batch adsorption experiments were performed in tap water (pH around 7.5) (Sturini et al., 2015b). MAR and ENR solutions were prepared with initial concentrations (C_0) ranging from 20 to 1800 mg L^{-1} and from 25 to 1000 mg L^{-1}, respectively.
50 mg of sepiolite were weighed into polypropylene centrifuge tubes, mixed with 10 mL of FQ solutions. pH values were adjusted around to 7.5 with HCl or NaOH and monitored every two hours until stabilized at the desired value. From the adsorption kinetics of the diluted antibiotic solutions, calculated by determining the concentrations of the solution at different contact times, it can be seen that equilibrium was reached after about 5 h. Nevertheless, when the batch adsorption experiments were performed, a contact time of 24 h, longer than the equilibration time, was employed in order to guarantee the system to reach the equilibrium state. Therefore, the tubes, wrapped with aluminium foils to prevent FQ light-induced decomposition, were shaken at 150 rpm for 24 h at room temperature (20 ± 1 °C). The suspensions were filtered through a 0.22 μm membrane filter for analysis. The equilibrium MAR and ENR concentrations (C_w) in the filtered solutions were measured by a UVmini-1240 UV-Vis spectrophotometer (Shimadzu Corporation) at the wavelengths of 290 and 270 nm, respectively. Calibrations with four standards at concentrations between 1 and 10 mg L^{-1} yielded optimal linearity (R^2 >0.9996). The quantification limits for MAR and ENR were in the range 0.4-0.5 mg L^{-1}. The MAR and ENR adsorbed amounts (C_s) were calculated from the difference between C_0 and C_w. All experiments were performed in triplicate with good reproducibility (RSD < 10%), while control solutions of each FQ with no sepiolite were also measured. No changes in FQ concentrations were detected in the control samples.

2.3. Sample preparation

For irradiation experiments, 0.1 g of sepiolite was fortified with MAR and ENR at a concentration of 10 mg g^{-1} of each drug, according to the batch procedure above described. After equilibration and filtration, the remaining pastes were dried at room temperature and homogeneously dispersed on glass Petri capsulae (∅ 8.5 cm, depth 2 cm) to obtain a monolayer (thickness below 1–2 mm). Afterwards, samples were exposed to natural sunlight (9.00 am–5.00 pm) during the summer (June–September), at temperatures ranging from 25 to 35 °C. The solar power ranged from 170 to 470 W m^{-2} (in the visible range) and from 8 to 30 W m^{-2} (in the UV), respectively. The flux was measured by means of a HD 9221 (Delta OHM) (450–950 nm) and of Multimeter (CO.FO.ME.GRA) (295–400 nm) radiometers. At regular intervals, each sample was extracted by microwave-assisted extraction (MAE); experiments were performed in triplicate.

For XRPD and FTIR-ATR analyses, sepiolite samples were separately enriched with 100 mg g^{-1} for MAR and ENR, concentration close to the maximum adsorption capacity. After 24 h equilibration, the suspensions were filtered and the remaining pastes were dried at room temperature.

2.4. Characterization of sepiolite samples

XRPD data were collected by using a Bragg–Brentano θ–θ diffractometer (PANalytical X-Pert Pro, Cu $K\alpha$ radiation, 40 kV and 40 mA) equipped with a real time multiple strip (RTMS) detector. Divergence and anti-scattering slits of 1/4° and 1/4°, respectively, were mounted in the incident beam pathway. The pathway of the diffracted beam included a Ni filter, a soller slit (0.04 rad) and antiscatter blade (5 mm). The virtual step scan of the measurement was 0.0167° 2θ. Si powder (NIST 640b) was added as standard.

Rietveld refinements aimed at determining the unit cells and quantitative phase analysis were performed using the GSAS software suite (Larson and Von Dreele, 2004) and its graphical interface EXPGUI (Toby, 2001). Backgrounds were subtracted by using shifted Chebyshev polynomials. The diffraction peak profiles were fitted with a pseudo-Voigt profile function with a Gaussian theta independent term a two Lorentzian terms. Scale factors relative to all phases present (see Results section) and unit-cell parameters of sepiolites were allowed to vary for all powder patterns. The morphology of the two sepiolite samples was studied by using a SEM TESCAN Mira 3 XMU equipped with a Schottky Field Emission gun (FE-SEM). Acceleration

159 voltage and working distance (WD) were 20 KV and 9.3 mm, respectively. Prior to FE-SEM examination,
160 powders were air-dried and coated with graphite under vacuum.
161 For IR spectroscopy, approximately 0.4 g of powder of each sample was pressed under vacuum to produce a
162 pellet. FTIR-ATR spectra were recorded at room temperature from 670 to 4000 cm^{-1} with a resolution of 4
163 cm^{-1} using a Thermo Scientific Nicolet iN10 MX micro-spectrometer. Every spectrum, recorded in ATR
164 with a liquid nitrogen cooled mercury cadmium telluride array detector, was calculated by Fourier
165 transformation of 256 interferometer scans and total scanning time of 90 seconds. A germanium
166 hemispherical internal reflection element (IRE) crystal with a diameter of 300 μm was used. The ATR
167 accessory is mounted on the X-Y stage of the FTIR microscope, and the IRE crystal makes contact with the
168 sample via a force lever with pressure of 2 Pa. A 37.7 × 37.7 μm aperture size was used.
169 BET surface areas of the sepiolite powders were determined by using a Gemini 2365 (Micromeritics).
170 Nitrogen of high purity grade was used as adsorbate. The samples were degassed under high vacuum on the
171 apparatus prior to the measurement. The degassing process was terminated when the vacuum pressure
172 decreased to 0.4 Pa. The molecular cross-section of nitrogen used in the data analysis was 0.1620 nm^2.
173
174 *2.5. Microwave-assisted extraction and chromatographic analyses*
175 A high performance instrument equipped with an infrared temperature control system, stirring and cooling
176 options (Discover SP® microwave system, CEM S.r.l., Cologno al Serio, Italy) was employed for MAE
177 from sepiolite samples enriched with FQs (see Section 2.3) before and after irradiation. Briefly, 10 mL of an
178 aqueous solution 100 mM TBAH-ACN (70:30) was added to 0.1 g of the adsorbed sepiolite in a Pyrex®
179 tube of 35 mL and introduced into the microwave cavity. After 2 min stirring, microwave irradiation (200
180 W) was performed to reach a temperature of 105°C, which was kept constant for 20 min. After cooling at
181 room temperature, the extract was centrifuged for 10 min at 4500 rpm, filtered (0.22 μm) and acidified with
182 H_3PO_4 (1:5) to pH 2.5 before HPLC-UV analysis.
183 The HPLC-UV system consisted of a Shimadzu (Milan, Italy) LC-20AT solvent delivery module equipped
184 with a DGU-20A3 degasser and interfaced with a SPD-20A UV detector. The analysis wavelength selected
185 was 275 nm. 20 μL of each sample was injected into a 250 × 4.6 mm, 5 μm Analytical Ascentis C18

(Supelco) coupled with a similar guard-column. The mobile phase was 25 mM H_3PO_4-ACN (85:15), at a flow rate of 1 mL min^{-1}. Instrumental quantification limits (IQLs) were in the range 0.1-0.2 mg L^{-1}.

3. Results and discussion

3.1 Sepiolites characterization

XRPD patterns of the natural and enriched sepiolite samples are shown in Fig. 1. Impurities are present in both samples: 1.6(1.0)% quartz and 1.1(0.5)% calcite in SP-1, and 12.0(2.5)% quartz, 5.8(0.4)% feldspar and 3.5(0.6)% calcite in SSE-16. Simply by visual inspection of the XRPD patterns, it is immediately evident how there are no differences after MAR and ENR adsorption. This is further confirmed by analysis of the refined unit-cell parameters of adsorbed sepiolites, which shows slightly differences with respect to those of the natural samples [a = 13.3758(38) Å; b = 27.0137(75) Å; c = 5.2507(15) Å for SP-1; a = 13.3956(41) Å, b = 26.8935(86) Å; c = 5.2431(17) Å for SSE16]. This may suggest that MAR and ENR are adsorbed superficially and do not enter the structure channels, although dimensions of the two molecules would fit (length (Å) 13.36 and 14.10, height (Å) 7.61 and 7.58 for MAR and ENR, respectively). This may be expected considering that no pre-treatment has been carried out on the sepiolites before adsorption experiments in order to remove water from structure channels.

Both sepiolite samples show fibrous morphologies (Fig. 2). The major part of the samples consists of fibres, which are often intertwined, giving in many cases flat tablets and forming a massive network. In both samples, fibre lengths are between 1 and 10 μm and hence can be classified as intermediate fibre sepiolites, according to the classification proposed by Sánchez del Río et al. (2011). The main differences in the two samples seem to be the thickness of the fibres, which are larger in SP-1, and their arrangement. In SP-1, elongate bundles of fibres are evident, while SSE16 displays flat tablets which are made up of tangled fibres. However, despite this different bundling, both samples present a closed porosity with fibres forming a dense mesh and compact texture.

The isotherms of adsorption of N_2 are similar in the two studied samples. They can be classified, according to the IUPAC classification, as Type II, which describes adsorption on macroporous adsorbents with strong

212 adsorbate-adsorbent interactions. The values of the BET surface area of the two samples are very similar as
213 well: 213(3) and 216(3) $m^2 g^{-1}$ for SP-1 and SSE-16, respectively.
214 Although the spectroscopic method alone is not sensitive enough to reveal the dynamics of the sorption
215 process, the FTIR-ATR spectra of sepiolite samples SP-1 and SSE16 before and after enrichment with MAR
216 or ENR were measured.
217 The spectra of sepiolites SP-1 and SSE16 show the characteristic band in the –OH stretching region,
218 corresponding to hydroxyls coordinated to the magnesium and to water in the structure (Frost et al., 2001).
219 No differences can be seen in the peaks relatives to Si-O and Al-O stretching modes of sepiolites after
220 enrichment with the antibiotics.
221 The FTIR-ATR spectra referred to clays enriched with MAR and ENR exhibited the main characteristic
222 peaks of adsorbed molecules in the region of 1800–1100 cm^{-1} (Yan et al., 2013) except for the 1690 cm^{-1}
223 peak. Comparing the FTIR-ATR spectrum of ENR to spectra of SP-1 and SSE16 enriched with ENR (Fig.
224 3), the peak corresponding to the C=O vibration from carboxylic acid oxygen and observed in control ENR
225 is not present in both FTIR-ATR spectra of enriched clays. Thus, the disappearing of the carboxylic acid
226 function is likely to be ascribable to a complexation between carboxylate and magnesium ions present on the
227 sepiolites surface, in agreement with literature (El-Shwiniy et al., 2013).
228
229 *3.2. Adsorption studies*
230 The adsorption isotherms of MAR and ENR were measured in order to define the adsorption capacity of the
231 two sepiolites in tap water (pH 7.5), because of its great similarity to surface water and its invariant
232 composition.
233 The adsorption isotherms were first interpreted using different models, i.e., Freundlich, Langmuir and SS-
234 logistic 1. The fitting parameters are listed in Table 1 and in Supplementary information.
235 The equation of Freundlich model is (Eq. (1)):
236 $$C_s = K_f C_w^n \qquad (1)$$
237 where K_f is the Freundlich constant (capacity factor), and n is the Freundlich exponent.
238 The equation of Langmuir model is (Eq. (2)):

$$C_s = \frac{SK_L C_w}{1 + K_L C_w} \quad (2)$$

where K_L is the Langmuir constant and S represents the total number of adsorption sites.

A further model was used to fit sigmoidal adsorption isotherms (Eq. (3))

$$C_s = \frac{C_{s\max}}{1 + e^{-A(C_w - F)}} \quad (3)$$

where C_s max is the maximum amount of molecule adsorbed, A is a coefficient indicating the efficiency of the adsorption mechanism, F represents the inflection point.

The adsorption profiles of MAR and ENR on SP-1 and SSE16 sepiolites show a similar sigmoidal trend, as depicted in Fig. 4. Adsorption capacities were specifically 132 and 121 mg g^{-1} for MAR and 112 and 93 mg g^{-1} for ENR on SP-1 and SSE16, respectively.

The isotherms parameters, obtained by the non-linear fitting performed with dedicated software (Origin®), are listed in Table 1. The good correlation coefficients (R^2) and chi-square (χ^2) show that the S-Logistic1 (Eq. (3)) model fits the results more accurately than Freundlich (Eq. (1)) and Langmuir (Eq. (2)). Fitting parameters from Freundlich and Langmuir models can be found in Supplementary material.

3.3. Photo-induced regeneration

It has been recently demonstrated that photodegradation of FQs is effective not only in aqueous solution but also in soil, montmorillonite and kaolinite (Sturini et al., 2012b; Sturini et al., 2015b). In this paper, the investigation has been extended to sepiolite. The experiments have been made only on SSE16, because of its similarity in terms of physical-chemical properties and sorption capacity as above demonstrated with SP-1 from Clay Mineral Society. The photodecomposition profiles of adsorbed MAR and ENR obtained on SSE16 sepiolite are shown in Fig. 5. The drugs showed a similar behaviour, as they are consistently degraded (>90%) in about 60 h when adsorbed on sepiolite. The FQs residual after irradiation is due to photodegradation, as it was experimentally verified by microwave-assisted extraction of sepiolite samples enriched with 10 mg g^{-1} FQs, *not* exposed to sunlight irradiation that provided quantitative recoveries of the two drugs (86%, RSD 10%, n=3). Moreover, no degradation was observed in control samples fortified with

each antibiotic (10 mg g^{-1}) and stored in the dark at room temperature for 1 month, and then submitted to MAE extraction. These findings excluded the potential biodegradation route that, in fact, it is inhibited by the high fixation rates of FQs to external sites of the matrix, in accordance with previous suggestions (Lai and Lin, 2009).

Experimental data are quite different from those previously obtained on soil (Sturini et al., 2012b), montmorillonite and kaolinite (Sturini et al., 2015b), where the incomplete degradation in up to 150 h was not due to soil particles not exposed to solar light, but rather to amounts of analyte differently located/complexed. The FQs photodegradation up to 90% on sepiolite indicates that the adsorption of MAR an ENR occurs on the external surface of sepiolite. These findings are in good agreement with the XRPD results that evidenced no structural modifications.

The complete photodegradation of FQs adsorbed on sepiolite suggests a possible re-usage of the adsorbent that can be regenerated by sunlight-induced decomposition of the adsorbed pollutants.

Conclusions

Sepiolite was, for the first time, investigated as sorbent phase for the potential removal of MAR and ENR fluoroquinolone drugs from water. The adsorption isotherms, fitted by the S-Logistic1 sigmoidal model, indicated sorption capacities of up to 132 mg g^{-1}. Adsorption occurred only on the external surface of the mineral and not in the intracrystalline microporosity, likely due to the interaction between the FQ carboxylic group and the Mg^{2+} ions present on the sepiolite surface, as indicated by XRPD and FTIR-ATR analyses. Solid-state photodegradation of the adsorbed antibiotics exposed to natural sunlight proved that the sorbent can be consistently photo-regenerated once recovered from water, thus showing the potential reuse of the “cleaned” sepiolite for further remediation of contaminated water.

Acknowlegments

The authors want to thank Prof. Massimo Setti for providing us with thesepiolites, and Dr. Elisa Rivagli and Dr. Simona Viti for theirexperimental support.

References

Andersson, M.I., MacGowan, A.P., 2003. Development of the quinolones. J. Antimicrob. Chemother. 51, 1–11.

Andreozzi, R., Raffaele, M., Nicklas, P., 2003. Pharmaceuticals in STP effluents and their solar photodegradation in aquatic environment. Chemosphere 50, 1319–1330.

Andreu, V., Blasco, C., Picó, Y., 2007. Analytical strategies to determine quinolone residues in food and the environment. Trends Anal. Chem. 26, 534–556.

Babić , S., Periša, M., Škorić , I., 2013. Photolytic degradation of norfloxacin, enrofloxacin and ciprofloxacin in various aqueous media. Chemosphere 91, 1635–1642.

Boxall, A.B.A., Johnson, P., Smith, E.J., Sinclair, C.J., Stutt, E., Levy, L.S., 2006. Uptake of veterinary medicines from soils into plants. J. Agr. Food Chem. 54, 2288–2297.

Brauner, K. and Preisinger, A., 1956. Struktur und Entstehung des Sepioliths. Mineralogy and Petrology, 6, 120–140.

De Bel, E., Dewulf, J., De Witte, B., Van Langenhove, H., Janssen, C., 2009. Influence of pH on the sonolysis of ciprofloxacin: biodegradability, ecotoxicity and antibiotic activity of its degradation products. Chemosphere 77, 291–295.

El-Shwiniy, W.H., El-Attar, M.S., Sadeek S.A., 2013. Metal complexes of Enrofloxacin part I: Preparation, spectroscopic, thermal analyses studies and antimicrobial evaluation. Journal of the Korean Chemical Society 57, 52–62.

318 Frost, R.L., Locos, O.B., Ruan, H., Kloprogge J.T., 2001. Near-infrared and mid-infrared spectroscopic
319 study of sepiolites and palygorskites. Vib. Spectrosc. 27, 1–13.
320
321 Ghahfarokhi, S.S.H., Landi, A., Khademi, H., Hojati, S., 2014. Removal of Cd^{2+} and Pb^{2+} ions from
322 aqueous solutions using Iranian natural zeolite and sepiolite. J. Environ. Stud. 40, 189–198.
323
324 Gianotti, V., Benzi, M., Croce, G., Frascarolo, P., Gosetti, F., Mazzucco, E., Bottaro, M., Gennaro, M.C.,
325 2008. The use of clays to sequestrate organic pollutants. Leaching experiments. Chemosphere 73, 1731–
326 1736.
327
328 Hartmann, A., Alder, A.C., Koller, T., Widmer, R.M., 1998. Identification of fluoroquinolone antibiotics as
329 the main source of umuC genotoxicity in native hospital water. Environ. Toxicol. Chem. 17, 377–382.
330
331 Kusari, S., Prabhakaran, D., Lamshöft, M., Spiteller, M., 2009. In vitro residual antibacterial activity of
332 difloxacin, sarafloxacin and their photoproducts after photolysis in water. Environ. Pollut. 157, 2722–2730.
333
334 Laera, G., Cassano, D., Lopez, A., Pinto, A., Pollice, A., Ricco, G., Mascolo, G., 2012. Removal of organics
335 and degradation products from industrial wastewater by a membrane bioreactor integrated with ozone or
336 UV/H_2O_2 treatment. Environ. Sci. Technol. 46, 1010–1018.
337
338 Lai, H.T., Lin, J.J., 2009. Degradation of oxolinic acid and flumequine in aquaculture pond waters and
339 sediments. Chemosphere 75, 462–468.
340
341 Larson, A.C. and Von Dreele, R.B., 2004. General structure analysis system (GSAS). Los Alamos National
342 Laboratory Report LAUR, 86-748.
343

Lester, Y., Avisar, D., Gozlan, I., Mamane H., 2011. Removal of pharmaceuticals using combination of UV/H_2O_2/O_3 advanced oxidation process. Water Sci. Technol. 64, 2230–2238.

Li Z.H., Hong H., Liao L., Ackley C.J., Schulz L.A., MacDonald R.A., Mihelich A.L., Emard S.M., 2011. A mechanistic study of ciprofloxacin removal by kaolinite. Colloid Surf. B 88, 339–344.

Li, Y., Niu, J., Wang, W., 2011. Photolysis of enrofloxacin in aqueous systems under simulated sunlight irradiation: kinetics, mechanism and toxicity of photolysis products. Chemosphere 85, 892–897.

Martucci, A., Pasti, L., Marchetti, N., Cavazzini, A., Dondi, F., Alberti, A., 2012. Adsorption of pharmaceuticals from aqueous solutions on synthetic zeolites. Micropor. Mesopor. Mater. 148, 174–183.

Murray, H.H., 1999. Applied clay mineralogy today and tomorrow. Clay Minerals 34, 39–49.

Nishimura, Y., Hori, Y., Takahashi, H., 1972. Structural change and adsorption character of sepiolite by heat treatment. Journal of the Clay Science Society of Japan 12, 102–108.

Prabhakaran, D., Sukul, P., Lamshöft, M., Maheswari, M.A., Zühlke, S., Spiteller, M., 2009. Photolysis of difloxacin and sarafloxacin in aqueous systems. Chemosphere 77, 739–746.

Quintelas, C., Figueiredo, H., Tavares, T., 2011. The effect of clay treatment on remediation of diethylketone contaminated wastewater: Uptake, equilibrium and kinetic studies. J. Hazard. Mater. 186, 1241–1248.

Reemtsma, T., Jekel, M., 2006. Organic Pollutant in the Water Cycle. Wiley-VCH, Weinheim.

Rizzo, L., Fiorentino, A., Anselmo, A., 2013. Advanced treatment of urban wastewater by UV radiation: effect on antibiotics and antibiotic-resistant E. coli strains. Chemosphere 92, 171–176.

Sánchez del Río, M., García-Romero, E., Suárez, M., da Silva, I., Fuentes-Montero, L., Martínez-Criado, G., 2011. Variability in sepiolite: Diffraction studies. Am. Mineral., 96, 1443–1454.

Sirtori, C., Zapata, A., Gernjak, W., Malato, S., Agüera, A., 2012. Photolysis of flumequine: identification of the major phototransformation products and toxicity measures. Chemosphere 88, 627–634.

Speltini, A., Sturini, M., Maraschi, F., Profumo, A., 2010. Fluoroquinolone antibiotics in environmental waters: sample preparation and determination. J. Sep. Sci. 33, 1115–1131.

Speltini, A., Sturini, M., Maraschi, F., Profumo, A., Albini, A., 2011. Analytical methods for the determination of fluoroquinolones in solid environmental matrices. Trends Anal. Chem. 30, 1337–1350.

Sturini, M., Speltini, A., Maraschi, F., Pretali, L., Ferri, E.N., Profumo, A., 2015a. Sunlight-induced degradation of fluoroquinolones in wastewater effluent: Photoproducts identification and toxicity. Chemosphere 134, 313–318.

Sturini, M., Speltini, A., Maraschi, F., Pretali, L., Profumo, A., Fasani, E., Albini, A., 2014. Environmental photochemistry of fluoroquinolones in soil and in aqueous soil suspensions under solar light. Environ. Sci. Pollut. Res. 21, 13215–13221.

Sturini, M., Speltini, A., Maraschi, F., Pretali, L., Profumo, A., Fasani, E., Albini, A., Migliavacca, R., Nucleo, E., 2012a. Photodegradation of fluoroquinolones in surface water and antimicrobial activity of the photoproducts. Water Res. 46, 5575–5582.

Sturini, M., Speltini, A., Maraschi, F., Profumo, A., Pretali, L., Fasani, E., Albini, A., 2010. Photochemical degradation of marbofloxacin and enrofloxacin in natural waters. Environ. Sci. Technol. 44, 4564–4569.

Sturini, M., Speltini, A., Maraschi, F., Profumo, A., Pretali, L., Fasani, E., Albini, A., 2012b. Sunlight-induced degradation of soil-adsorbed veterinary antimicrobials marbofloxacin and enrofloxacin. Chemosphere 86, 130–137.

Sturini, M., Speltini, A., Maraschi, F., Rivagli, E., Pretali, L., Malavasi, L., Profumo, A., Fasani, E., Albini, A., 2015b. Sunlight photodegradation of marbofloxacin and enrofloxacin adsorbed on clay minerals. J. Photochem. Photobiol. A: Chem. 299, 103–109.

Suárez, M., and García-Romero, E., 2012. Variability of the surface properties of sepiolite. Appl. Clay Sci. 67, 72–82.

Sukul, P., Lamshöft, M., Kusari, S., Zühlke, S., Spiteller, M., 2009. Metabolism and excretion kinetics of ^{14}C-labeled and non-labeled difloxacin in pigs after oral administration, and antimicrobial activity of manure containing difloxacin and its metabolites. Environ. Res. 109, 225–231.

Toby, B.H., 2001 EXPGUI, A graphical user interface for GSAS. J. Appl. Crystallogr., 34, 210–213.

Van Doorslaer, X., Demeestere, K., Heynderickx, P.M., Van Langenhove, H., Dewulf, J., 2011. UV-A and UV-C induced photolytic and photocatalytic degradation of aqueous ciprofloxacin and moxifloxacin: reaction kinetics and role of adsorption. Appl. Catal. B – Environ. 101, 540–547.

Vasconcelos, T.G., Henriques, D.M., König, A., Martins, A.G., Kümmerer, K., 2009. Photo-degradation of the antimicrobial ciprofloxacin at high pH: identification and biodegradability assessment of the primary by-products. Chemosphere 79, 487–493.

424 Vieno, N.M., Härkki, H., Tuhkanen, T., Kronberg, L., 2007. Occurrence of pharmaceuticals in river water
425 and their elimination in a pilot-scale drinking water treatment plant. Environ. Sci. Technol. 41, 5077–5084.
426
427 Wang, Y.Q.J., Mo, C.H., Li, Y.W., Gao, P., Tai, Y.P., Zhang, Y., Ruan, Z.L., Xu, J.W., 2010. Determination
428 of four fluoroquinolone antibiotics in tap water in Guangzhou and Macao. Environ. Pollut. 158, 2350–2358.
429
430 Yan, W., Zhang, J., Jing, C., 2013. Adsorption of Enrofloxacin on montmorillonite: Two-dimensional
431 correlation ATR/FTIR spectroscopy study. J. Colloid Interface Sci. 390, 196–203.
432
433 Ye, Z., Weinberg, H.S., 2007. Trace analysis of trimethoprim and sulfonamide, macrolide, quinolone, and
434 tetracycline antibiotics in chlorinated drinking water using liquid chromatography electrospray tandem mass
435 spectrometry. Anal. Chem. 79, 1135–1144.
436
437
438 **Figure captions**
439 **Fig. 1.** XRPD patterns for the crude sepiolite samples and after adsorption: (a) SP-1; (b) SSE16.
440 **Fig. 2.** FE-SEM images of crude sepiolites: (a) SP-1; (b) SSE16.
441 **Fig. 3.** FTIR-ATR of ENR, of crude sepiolites (SP-1, SSE16) and of sepiolites (SP-1, SSE16) enriched with
442 ENR.
443 **Fig. 4.** Adsorption isotherms of MAR on (a) SP-1 and on (b) SSE16, and of ENR on (c) SP-1 and on (d)
444 SSE16.
445 **Fig. 5.** Degradation profiles obtained under solar light for MAR (◇) and ENR (○) adsorbed on SSE16.
446
447
448 **Table title**
449 **Table 1.** Parameters obtained by fitting the experimental data of MAR and ENR adsorption on sepiolites to
450 the S-logistic 1 model.

Figure 1

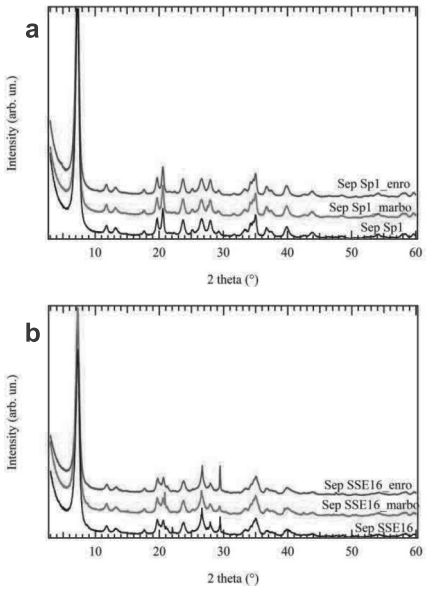
a
Intensity (arb. un.)
Sep Sp1_enro
Sep Sp1_marbo
Sep Sp1
10
20
30
40
50
60
2 theta (°)
b
Intensity (arb. un.)
Sep SSE16_enro
Sep SSE16_marbo
Sep SSE16
10
20
30
40
50
60
2 theta (°)

Figure 2

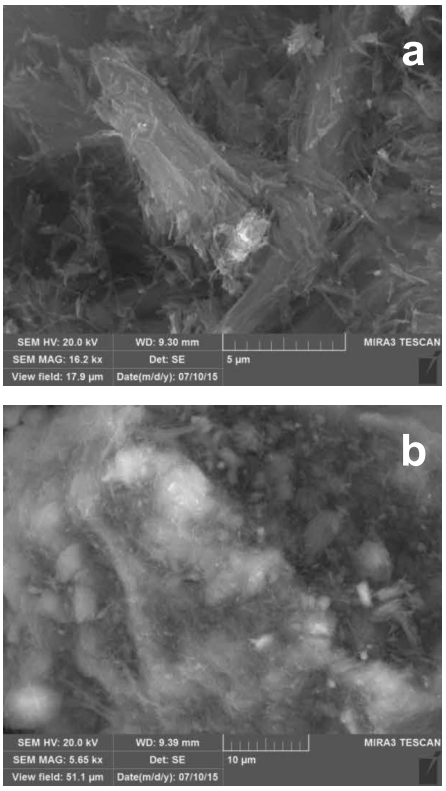
a
SEM HV: 20.0 kV
WD: 9.30 mm
MIRA3 TESCAN
SEM MAG: 16.2 kx
Det: SE
5 µm
View field: 17.9 µm
Date(m/d/y): 07/10/15
b
SEM HV: 20.0 kV
WD: 9.39 mm
MIRA3 TESCAN
SEM MAG: 5.65 kx
Det: SE
10 µm
View field: 51.1 µm
Date(m/d/y): 07/10/15

Figure 3

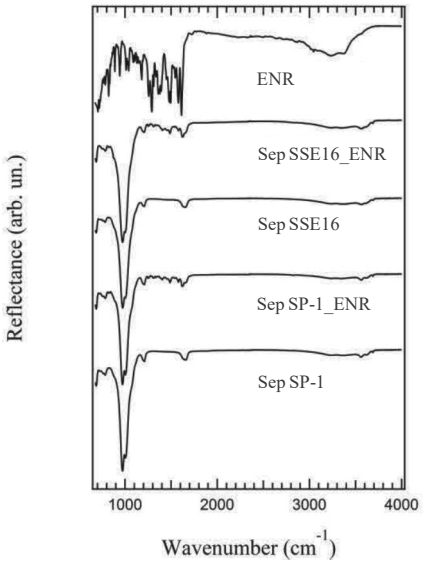
ENR
Sep SSE16_ENR
Sep SSE16
Sep SP-1_ENR
Sep SP-1
Reflectance (arb. un.)
1000
2000
3000
4000
Wavenumber (cm-1)

Figure 4

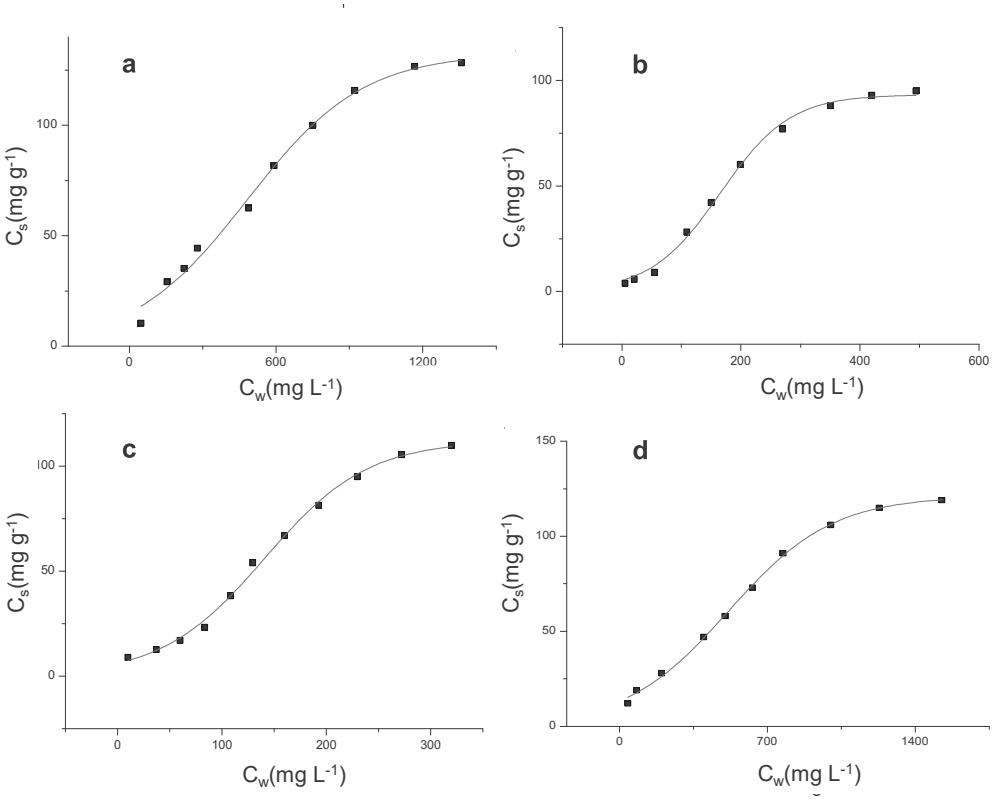
a
b
c
d
C_s(mg g^{-1})
C_w(mg L^{-1})
0
50
100
600
1200
200
400
600
300
150
700
1400

Figure 5

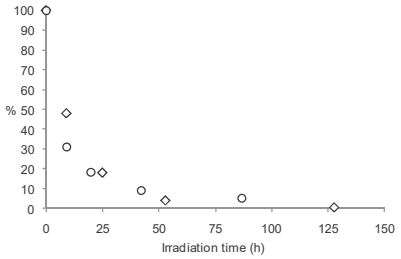
100
90
80
70
60
% 50
40
30
20
10
0
0
25
50
75
100
125
150
Irradiation time (h)

Table 1
Click here to download Table: Table 1.doc

Sigmoidal model (S-Logistic 1)						
FQ	sepiolite	R^2	χ^2	$C_{s\,max}$ (mg g^{-1})	A	F
MAR	SP-1	0.9907	17.3	132 ± 4	0.0042 ± 0.0003	482 ± 24
	SSE16	0.9983	2.8	121 ± 1	0.0041 ± 0.0001	516 ± 11
ENR	SP-1	0.9966	4.9	112 ± 2	0.020 ± 0.001	141 ± 3
	SSE16	0.9959	5.6	93 ± 2	0.017 ± 0.001	165 ± 5

Supplementary Material

Click here to download Supplementary Material: Supplementary material.doc